Controlled synthesis of MnO_2/CNT nanocomposites for supercapacitor applications

D. Z. W. Tan, H. Cheng, S. T. Nguyen and H. M. Duong*

In this work, manganese oxide (MnO_2)/carbon nanotube (CNT) nanocomposites have been prepared as electrode materials for supercapacitor applications. The materials were synthesised using a traditional and facile chemical deposition method. Effects from CNT amounts, synthesis time, pH value and CNT treatment using nitric acid have been thoroughly investigated. It was found that the sample synthesised for 3 h at pH 5 had achieved the best performance with a specific capacitance of 115 F g^{-1} at a discharge rate of 0·5 A g^{-1}. A capacitance retention of 95% after 1000 cycles has been observed for the sample synthesised in the neutral environment. We believe that findings from this work will pave a road for nanostructured MnO_2/CNT composites with better performance in energy storage applications.

Keywords: CNT composites, Controlled synthesis, Manganese oxides, Supercapacitor

This paper is part of a special issue on functional materials for electrochemical energy storage

Introduction

Nowadays, the depletion of fossil fuels and global warming have driven the search for renewable sustainable energies. Methods of harvesting energy include solar, hydroelectric, wind, geothermal and nuclear energy have been developed.[1] However, harvesting sustainable energy is only one part of the solutions. Methods of managing and storing the energy have also been investigated in order to efficiently utilise them to cater the market requirements. One way of storing energy is via supercapacitors. A supercapacitor is basically an electrochemical energy storage device incorporating the merits of batteries and physical capacitors capable of storing a substantial amount of energy for use at fast charge/discharge rate. Some applications of supercapacitors include, but are not limited to, stabilising power supplies in fluctuating loads, emergency shutdown power for low power equipment, energy storage for solar powered street lamps and energy recovery of braking energy in buses, trams and light rail.[2]

Supercapacitors can be generally classified into two types based on their working mechanisms.[3] Electrochemical double layer capacitors work on an electrostatic storage of electricity by the separation of charge between the electrode and electrolyte. While the other type is pseudocapacitors, which utilise the transfer of electrons from redox reactions with adsorbed ions from the electrolyte, intercalation of atoms in the layer lattice or the deposition of metal in surface lattice sites to get a reversible Faradaic charge transfer.[4]

Currently, various materials have been investigated as electrodes of pseudocapacitors including manganese oxide,[5–7] nickel oxide/hydroxide,[8–10] cobalt oxide/hydroxide[11–14] and conducting polymers.[15–17] Among them, great attention was paid to manganese oxides for their high theoretical capacitance, natural abundance and low toxicity.[18,19] Compared with nickel oxides/hydroxides and cobalt oxides/hydroxides, MnO_2 has a wider working potential near 1 V, leading to a higher energy density. It is also believed that the layered or tunnelled crystal structures of the MnO_2 can facilitate ion diffusion inside the bulk materials much better than the spinal structure of most copper ferrite materials.[20] Unfortunately, manganese oxides suffer from a low electric conductivity (10^{-4}–10^{-6} S cm^{-1}),[21] which impairs their power performance. Addressed to this issue, carbon nanotubes (CNTs), possessing high electrical conductivity and mechanical strength,[22–25] have been incorporated to manganese oxide to further enhance their electrical conductivity.

Many approaches have been applied to prepare MnO_2/CNT composites for supercapacitor applications. Ma *et al.* have applied a simple chemical bath method to coat CNTs with a thin layer of MnO_2 based on the redox reaction between the CNTs and the permanganate, and a capacitance of ~250 F g^{-1} has been achieved at 1 A g^{-1}.[26] However, the test environment with Li foil as the counter electrode and $LiClO_4$ (solved in propylene carbonate) as electrolyte makes it resemble a lithium battery rather than a supercapacitor. A hydrothermal method has also been applied by Teng *et al.* to synthesise MnO_2/CNT composites, which could achieve 264 F g^{-1} at 1 mA cm^{-2}. More interestingly, by taking advantage of a nanocrystal nucleation, Xia *et al.*

Department of Mechanical Engineering, National University of Singapore, 9 Engineering Drive, Singapore 117576, Singapore

*Corresponding author, mpedhm@nus.edu.sg

Received 28 May 2014; accepted 19 June 2014
DOI 10.1179/1753555714Y.0000000175

has designed a core/shell structure with MnO_2 nanoflakes coated on CNT cores to deliver a capacitance as high as 223 F g^{-1} at 10 mV s^{-1}.[27] Furthermore, a microwave assisted reaction was developed to synthesise the composite to reach 944 F g^{-1} based on the mass of MnO_2 along. However, if considered the total mass of composite, only 141 F g^{-1} was achieved.[28] Wang *et al.* has used a chemical vapour deposition method to first grow CNTs on the stainless steel (SS) meshes and then synthesised MnO_2 via a cathodic deposition. The coated SS meshes were then directly used as working electrodes without any polymer binder and a specific capacitance of 356 F g^{-1} was achieved at 2 mV s^{-1}.[29] With the utilisation of an anodic aluminium oxide templates, Reddy *et al.* have prepared multisegmented Au–MnO_2/CNT hybrid coaxial arrays, resulting in a specific capacitance of 68 F g^{-1} based on the total mass of materials and current collectors.[30] By electrodepositing MnO_2 on CNT coated cotton sheets, Hu *et al.* have achieved a capacitance of 410 F g^{-1}.[31]

For the MnO_2 synthesis based on the direct reaction between the CNTs and permanganate, synthesis conditions such as CNT amounts, reaction time, solution acidity and CNT oxidation degree will affect the properties of the prepared materials, which have not yet been thoroughly investigated. Therefore, in this work, different synthesis conditions have been varied to tune the MnO_2/CNT composite properties in order to achieve a better performance.

Experimental

Materials

Multiwalled CNTs, 10–20 nm in diameter and 5–15 μm in length, were purchased from Shenzhen Nanotechnologies Port Co., Ltd. Potassium permanganate was purchased from Sigma-Aldrich Chemical, hydrochloric acid was obtained from Merck and nitric acid was obtained from Fluka. All chemicals were used as received without further purifications.

Sample preparation

For the oxidisation of the CNTs, 500 mg CNTs were dispersed into the nitric acid with different concentrations (10, 20, 30 and 40% and 65 wt-%) under sonication for 30 min. Then, the dispersion was heated with a condenser at 120°C for 6 h. Next, the dispersion was washed with copious deionised water by centrifugation until its pH value reached 7. The treated CNTs were then collected using vacuum filtration and dried at 60°C in an oven overnight.

The MnO_2/CNT nanocomposites were synthesised via a direct redox reaction between the CNTs and $KMnO_4$. For the standard samples, the treated CNTs were dispersed in 50 mL deionised water by probe sonication for 30 min followed by bath sonication for another 30 min. Three hundred milligrams $KMnO_4$ was then added to the CNT dispersion. For samples synthesised under different acidities, certain amount of HCl was used to tune the initial pH value before the reaction. The mixture was then heated at 70°C for 3 h before being collected via vacuum filtration. Subsequently, the collected sample was rinsed with distilled water and ethanol before being dried overnight in an oven at 60°C. Synthesis parameters such as CNT amounts, synthesis time, pH value and the CNT oxidation degree have been varied to investigate their effects on the products as seen in Table 1.

Characterisations

Crystal structures of the as synthesised samples were characterised by powder X-ray diffraction (XRD) using a Shimazu XRD 6000 X-ray diffractometer equipped with Cu K_α radiation (k=1·5418 Å). The morphologies of composites were examined by a field emission scanning electron microscopy (Hitachi S4300 FESEM). Transmission electron microscopy (TEM) was performed on a JEOL 3010 to further investigate the microstructures of the composites. Thermogravimetric analysis was conducted in ambient atmosphere at a heating rate of 10°C min^{-1} to 1000°C on a Shimadzu DTG-60H thermal analyser.

Electrochemical measurements

Working electrodes were prepared by mixing 90 wt-% active materials (MnO_2/CNT composites), 5 wt-% acetylene black and 5 wt-% polytetrafluoroethylene binder to form a paste and spread onto nickel foams. The working electrodes were then dried at 60°C for overnight and compressed under a pressure of 0·5 metric tons. Typically, 4–6 mg working materials (including polytetrafluoroethylene and carbon additives) were loaded on electrodes. The electrochemical performance of the electrodes was characterised by cyclic voltammetry (CV) at 5, 10, 20, 30, 40 and 50 mV s^{-1} from 0 to 1 V(Ag/AgCl) and galvanostatic charge/discharge (GCD) at 0·5, 1, 2, 3 and 4 A g^{-1} from 0 to 0·9 V(Ag/AgCl). All the electrochemical tests were conducted in 1 mol L^{-1} Na_2SO_4 with a three-electrode configuration using a Solartron 1470E electrochemical workstation with a Pt foil as the counter electrode and Ag/AgCl as the reference electrode. The specific capacitance was calculated using the following equation

From CV

$$C_s = \frac{\int I \mathrm{d}V}{2ms\Delta V} \tag{1}$$

From GCD

$$C_s = \frac{I\Delta t}{m\Delta V} \tag{2}$$

where C_s is the specific capacitance (F g^{-1}), I is the discharge current (A), ΔV is the potential window (V),

Table 1 Synthesis conditions of MnO_2/CNT composites

CNT amount/mg	Synthesis time/h	pH value	HNO_3 concentration/wt-%
40	1	1	0
70	3	3	10
100	5	5	20
130	7	7	30
Standard sample: pristine CNTs: 100 mg; reflux time: 3 h at pH –7			40
			65

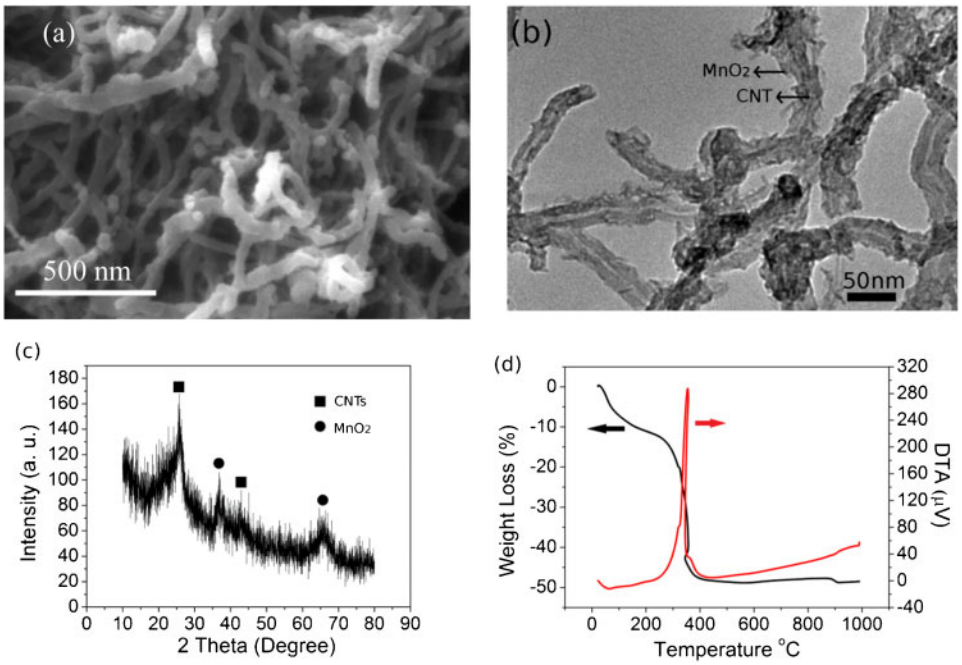

a FESEM images; *b* TEM images; *c* XRD patterns; *d* thermogravimetric analysis curve

1 Characterisation of standard samples

Δt is the discharge time (s), s is the scanning rate (V s^{-1}) in CV test and m is the mass (g) of testing materials including the acetylene carbon and polymer binder.

Results and discussion

The materials have been synthesised using a facile chemical deposition method[32] based on the reaction between CNTs and potassium permanganate. The growth of the MnO_2 mainly originates from the redox reaction between the permanganate and CNTs.

Figure 1*a* shows the SEM images of the sample synthesised 3 h without the addition of HCl using 100 mg pristine CNTs (standard sample). As can be seen, the nanotubes with a thin layer coating of the MnO_2 slightly tangle together with diameter about 30–50 nm. The growing mechanism can be easily explained by the following equation[33]

$$4MnO_4^- + 3C + H_2O \rightarrow 4MnO_2 + CO_3^{2-} + 2HCO_3^- \quad (3)$$

The permanganate is generally believed to react with defect sites of CNTs and give the crystal nucleation.[33] According to Jin *et al.*, such kind of reaction is not a simple local but a microelectrochemical cell reaction. The defect sites such as nanotube ends will donate the electrons which transfer along the CNTs to reduce the permanganate at the other sites. Such kind of reaction is capable of promoting the continuous growth of the manganese oxides. Based on the SEM observation of our samples (Fig. 1*a*), the inhomogeneity of MnO_2 coating with aggregations is easily observed at the nanotube ends. Unlike the CNTs treated by concentric sulphuric acid together with nitric acid in the work of Jin *et al.*,[33] the standard sample presented here possesses limited defects on the CNTs in the absence of the strong acid treatment. From this perspective, we propose that both local redox and microelectrochemical cell reaction occur during the synthesis, which results in an inhomogeneous coating of MnO_2. This speculation was also confirmed by TEM images with inhomogeneous nano-MnO_2 flakes coated on the nanotube surface (Fig. 1*b*).

The XRD data given in Fig. 1*c* help to reveal the crystal structures of the synthesised MnO_2/CNT composites. The peaks at 26 and 44° can be attributed to the CNTs, while those at 37 and 66° come from the crystal planes of (11*l*) and (02*l*) in birnessite MnO_2, which is consistent with the literature.[34] Compared with the peaks of the CNTs, the intensity of the MnO_2 peaks is much lower, indicating their poor crystallinity. To further determine the MnO_2 content in the nanocomposite, the thermogravimetric analysis was also performed in the ambient atmosphere as seen in Fig. 1*d*. The initial weight drop of 10% below 200°C is due to the loss of the adsorbed and interlayer water.[35] The following sharp decrease ~300°C originates from the oxidation of CNTs in air.[36] Based on the thermogravimetric analysis, the MnO_2 content is estimated to be 53 wt-% in the composite.

Figure 2*a* presents the CV curve of the standard samples at different scanning rates. A rectangular shape with small broad peaks can be easily indentified, indicating ideal capacitance behaviour. The capacitance originates from the valence changes of the manganese described by the following equation[18,19]

$$MnO_2 + xNa^+ + yH^+ + (x+y)e- \rightleftharpoons MnOONa_xH_y(surface) \quad (4)$$

The redox reaction contributing to the capacitance can proceed at or near the surface of materials at a continuous expanded window,[18] which gives a rectangular shape, different from the sharp peaks observed with nickel oxide/hydroxide and cobalt oxide/hydroxide.[37–40] With the increase in the scanning rate, CV curves distort due to a slow ion transportation and limited electrical conductivity of the composites.

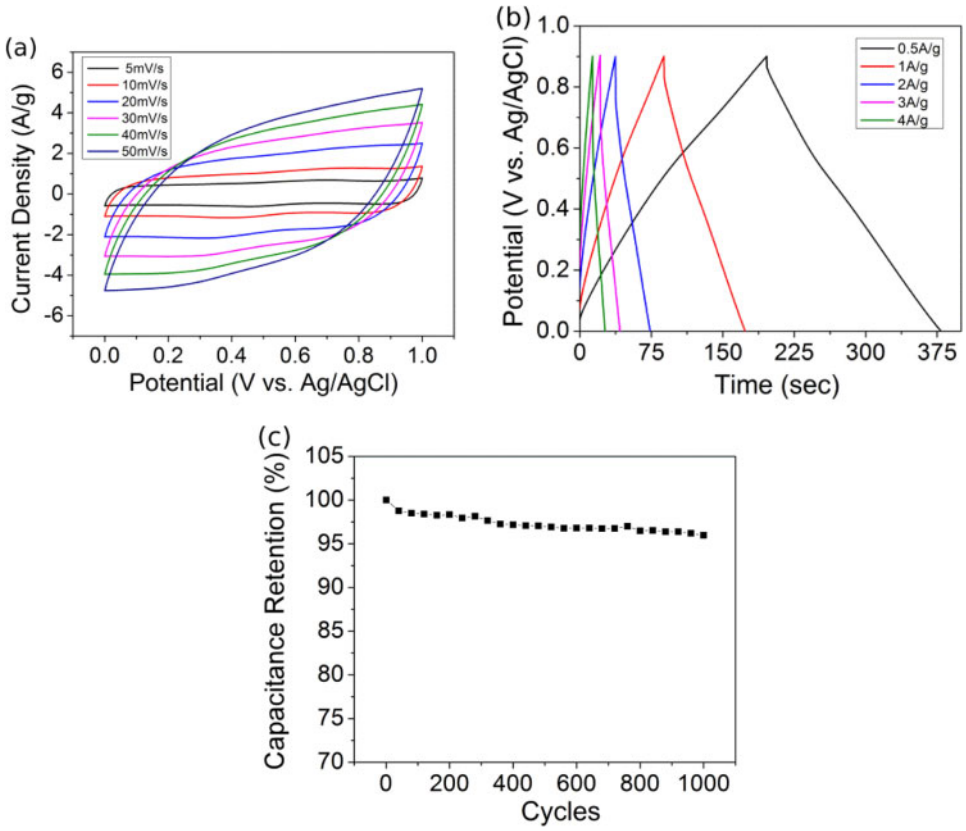

a CV curves at different scan rates; *b* GCD curves at different discharge rate; *c* cycling performance

2 Electrochemical characterisations of standard samples

Figure 2*b* presents linear charge/discharge curves originating from an ideal capacitance performance. The specific capacitance calculated from the 0·5, 1, 2, 3 and 4 A g^{-1} are 106, 102, 94, 89 and 83 F g^{-1} based on the mass of the whole composite (including polytetrafluoroethylene binder and carbon additive) and 222, 219, 197, 187 and 174 F g^{-1} based on the MnO_2 alone respectively. The cycling stability has also been tested over 1000 cycles of GCD at 1 A g^{-1} with retention above 95% (Fig. 2*c*).

To better understand the growing mechanism and to tune the electrochemical performance of the MnO_2/CNT nanocomposite, composites with different pristine CNT contents have been investigated. During the materials preparation, the synthesis time was fixed at 3 h and no HCl was added to tune the pH value. As can be seen in Fig. 3*a*, the sample of 100 mg has the largest enclosed area, indicating the highest specific capacitance. The further increase in the CNTs may cause a severe entanglement, which impairs their electrochemical performance, and the decrease in the CNT amount will either decrease the total mass of the MnO_2 coated due to a reduced surface area there or a lower conductivity. As a result, the specific capacitance decreases.

Besides the CNT amounts, synthesis time is also a key element in determining the composite performance, which has been investigated with the fixed amount of CNTs at 100 mg. From the CV and GCD curves presented in Fig. 4*a* and *c*, we find that 3 h are the optimised reaction period for the synthesis of the composites. The materials synthesised for 1 h has an apparent low capacitance because of an uncompleted reaction. While the increase in the synthesis time leads to a better performance. However, with the further increase in the refluxing time, the capacitance drops since the increased thickness of the MnO_2 coating on the CNTs blocks small channels for the ion diffusion and thus impairs the electrochemical performance. The effects of the synthesis time can also be observed from the solution colour change during the synthesis. For materials synthesised for 1 h, the solution still kept a dark purple after the heating process, indicating an uncompleted reaction. While with an increased synthesis time to 7 h, the solution becomes light brown due to the completed consumption of the permanganate

Since the growing reaction is based on the redox couple between the CNT defects and permanganate, the acidity of the solution will affect the materials performance. An increase in the acidity of the solution will enhance the oxidising ability of permanganate but at the same time weaken the reducing capability of the carbon defects in the nanotubes.[33] From this perspective, there should be an optimised pH value of the composite synthesis. Here, we study the effects of the solution acidity using different hydrochloric acid concentrations to tune the pH value. From the electrochemical characterisation, the composite synthesised at pH 5 has optimised properties (as seen in Fig. 5*b* and *d*). The further increase in initial pH value will suppress the oxidising ability of $KMnO_4$, while the decrease in pH value will lower the reducing ability of carbon defects.

So far, we found the MnO_2/CNT composite with 100 mg CNT synthesised at pH 5 for 3 h gives the best results. To get a better dispersion of CNTs for the growth of MnO_2, we also treat CNTs using nitric acid with different concentrations to slightly oxidise them in order to improve the wettability. As can be seen from the CV curves in Fig. 6*a*, with the increase in

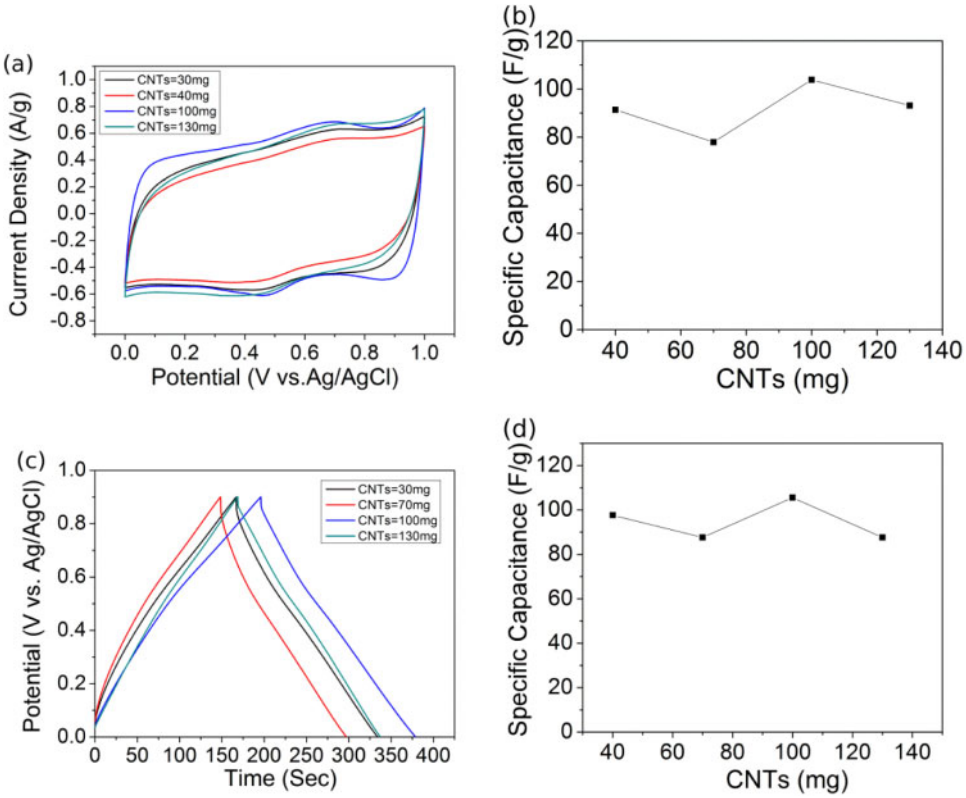

a CV at 5 mV s^{-1} with different CNT additions; *b* specific capacitance calculated from CV curves; *c* GCD at 0·5 A g^{-1} with different CNT additions; *d* specific capacitance calculated from GCD curves

3 Effects from different CNTs

the HNO_3 concentration, the composites containing treated CNTs exhibit sharper anodic peaks ~0·7 V coming from the contribution of the functional groups[41] of the treated CNTs. However, the capacitance undergoes a sudden drop after the HNO_3 treatments. We propose that this is because the initial treatment of HNO_3 causes a great number of carbon disorders and brings a dramatic conductivity change. With the treatment from higher concentrated HNO_3, the capacitance increases a little due to the better

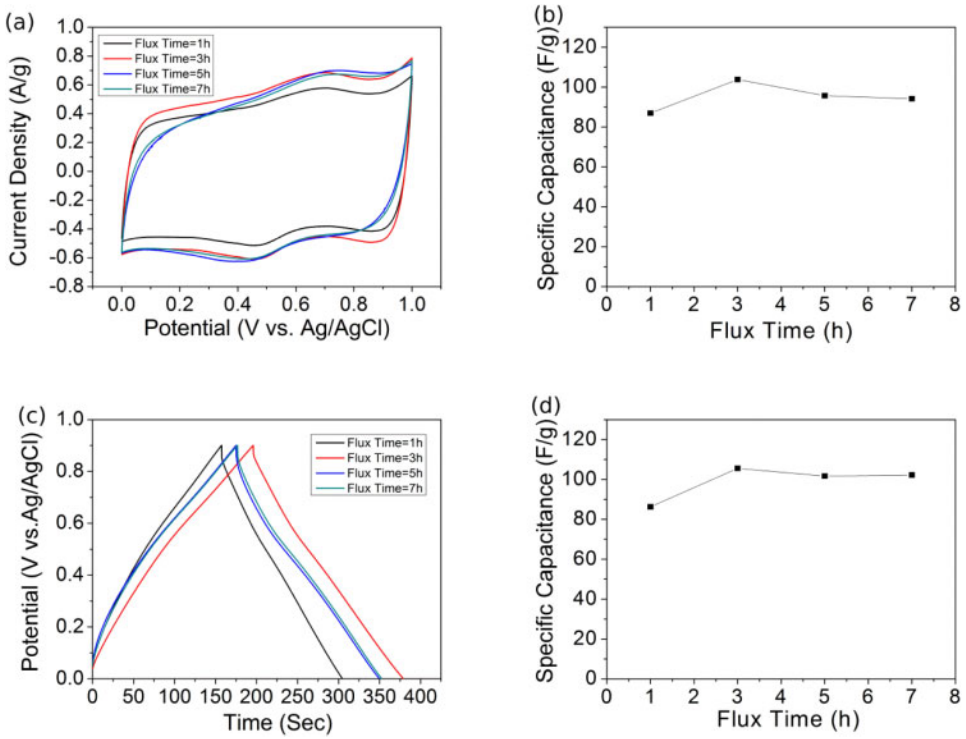

a CV at 5 mV s^{-1} with different flux times; *b* specific capacitance calculated from CV curves; *c* GCD at 0·5 A g^{-1} with different flux times; *d* specific capacitance calculated from GCD curves

4 Effects from different flux times

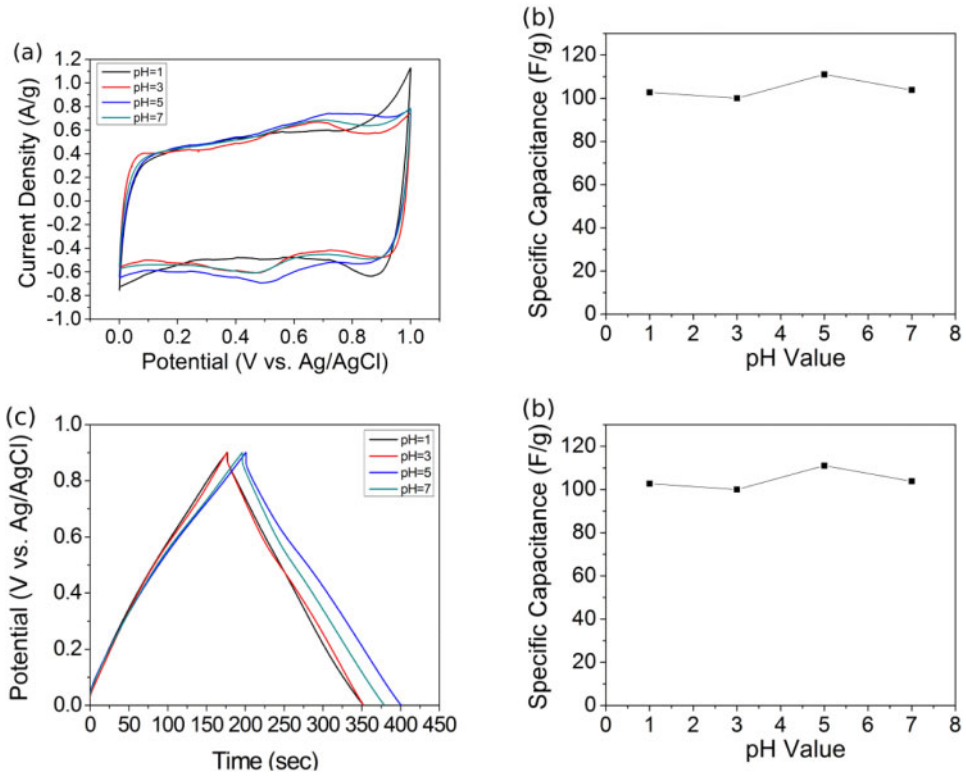

a CV at 5 mV s^{-1} with different pH values; *b* specific capacitance calculated from CV curves; *c* GCD at 0·5 A g^{-1} with different pH values; *d* specific capacitance calculated from GCD curves

5 Effects from different pH values

dispersion with the negative charged CNTs. With the increase in the HNO_3 concentration over 30%, however, the positive effects from the better dispersion cannot compensate the conductivity drop and results in a decreased capacitance.

Conclusions

In this paper, MnO_2/CNT composites were successfully synthesised using a facile redox reaction between $KMnO_4$ and CNTs. As results, a thin layer of birnessite

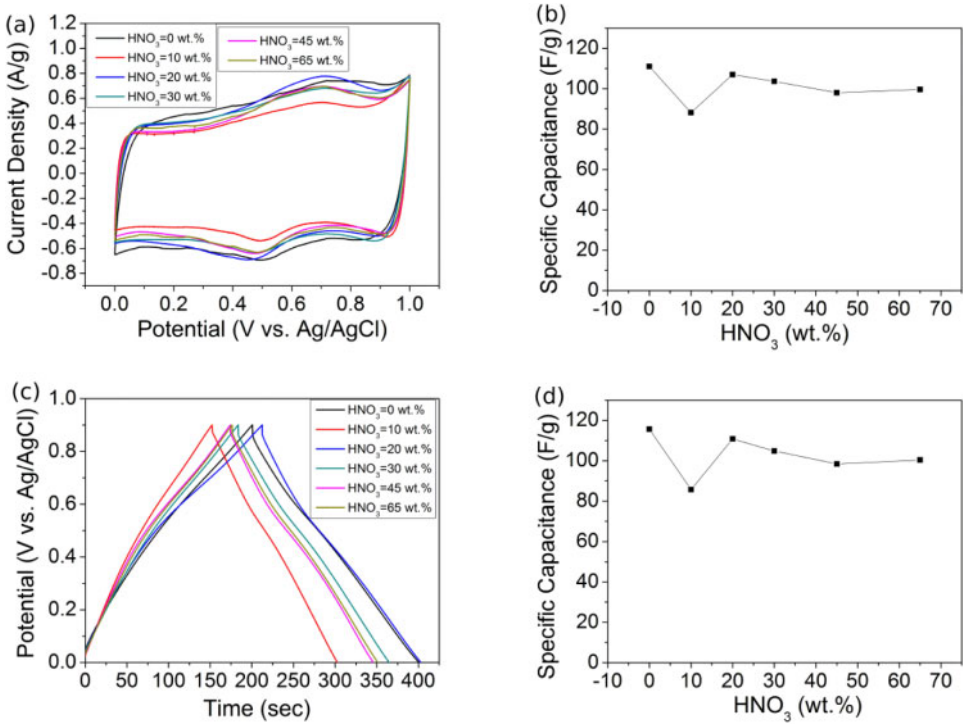

a CV at 5 mV s^{-1} with different HNO_3 concentrations; *b* specific capacitance calculated from CV curves; *c* GCD at 0·5 A g^{-1} with different HNO_3 concentrations; *d* specific capacitance calculated from GCD curves

6 Effects from CNTs treated by different concentrated HNO_3

type MnO_2 was coated onto CNTs. The prepared composite used as electrodes for supercapacitor has achieved a good cycling retention over 95%. After varying different synthesis conditions, it is found that the composite synthesised with 100 mg of CNT and a reflux time of 3 h at pH 5 showed the highest specific capacitance of 115 F g^{-1}.

Acknowledgements

This work is supported by the Singapore PSF A*STAR Grant on 'Advanced Energy Devices Using Carbon Nanotube Aerogels' (R265-000-424-305/331). We also would like to take this opportunity to thank Professor L. Li for his great help and discussion.

References

1. Z. Yang, J. Zhang, M. C. W. Kintner-Meyer, X. Lu, D. Choi, J. P. Lemmon and J. Liu: 'Electrochemical energy storage for green grid', *Chem. Rev.*, 2011, **111**, 3577–3613.
2. R. Kötz and M. Carlen: 'Principles and applications of electrochemical capacitors', *Electrochim. Acta*, 2000, **45**, 2483–2498.
3. P. J. Hall, M. Mirzaeian, S. I. Fletcher, F. B. Sillars, A. J. R. Rennie, G. O. Shitta-Bey, G. Wilson,A. Cruden, R. Carter: 'Energy Storage in Electrochemical Capacitors: *Energy Environ. Sci*. 2010, **3**, 1238–1251.
4. C. Lokhande, D. Dubal and O. Joo: 'Metal oxide thin film based supercapacitors', *Curr. Appl. Phys.*, 2011, **11**, 255–270.
5. H. Xia, J. Feng, H. Wang, M. O. Lai and L. Lu: 'MnO_2 nanotube and nanowire arrays by electrochemical deposition for supercapacitors', *J. Power Sources*, 2010, **195**, 4410–4413.
6. O. Ghodbane and J. L. Pascal and F. Favier: 'Microstructural effects on charge-storage properties in MnO_2-based electrochemical supercapacitors', *ACS Appl. Mater. Interfaces*, 2009, **1**, 1130–1139.
7. D. Yan, Z. Guo, G. Zhu, Z. Yu, H. Xu and A. Yu: 'MnO_2 film with three-dimensional structure prepared by hydrothermal process for supercapacitor', *J. Power Sources*, 2012, **199**, 409–412.
8. H. Wang, Q. Pan, X. Wang, G. Yin and J. Zhao: 'Improving electrochemical performance of NiO films by electrodeposition on foam nickel substrates', *J. Appl. Electrochem.*, 2009, **39**, 1597–1602.
9. Y. Q. Zhang, X. H. Xia, J. P. Tu, Y. J. Mai, S. J. Shi, X. L. Wang and C. D. Gu: 'Self-assembled synthesis of hierarchically porous NiO film and its application for electrochemical capacitors', *J. Power Sources*, 2012, **199**, 413–417.
10. Y. Khan, S. Hussain, F. Söderlind, P. O. Käll, M. A. Abbasi and S. K. Durrani: 'Honeycomb β-$Ni(OH)_2$ films grown on 3D nickel foam substrates at low temperature', *Mater. Lett.*, 2012, **69**, 37–40.
11. Q. Yang, Z. Lu, X. Sun and J. Liu: 'Ultrathin Co_3O_4 nanosheet arrays with high supercapacitive performance', *Sci. Rep.*, 2013, **3**, 3537.
12. S. K. Meher and G. R. Rao: 'Ultralayered Co_3O_4 for high-performance supercapacitor applications', *J. Phys. Chem C*, 2011, **115C**, 15646–15654.
13. Y. Tang, Y. Liu, S. Yu, S. Mu, S. Xiao, Y. Zhao and F. Gao: 'Morphology controlled synthesis of monodisperse cobalt hydroxide for supercapacitor with high performance and long cycle life', *J. Power Sources* 2014, **256**, 160–169.
14. H. Cui, M. Wang, W. Ren and Y. Zhao: 'Low temperature synthesis of high electrochemical performance Co_3O_4 nanoparticles for application in supercapacitor', *Funct. Mater. Lett.*, 2014, **07**, 1450002.
15. S. Patra and N. Munichandraiah: 'Supercapacitor studies of electrochemically deposited PEDOT on stainless steel substrate', *J. Appl. Polym. Sci.*, 2007, **106**, 1160–1171.
16. L. Liu, Y. Zhao, Q. Zhou, H. Xu, C. Zhao and Z. Jiang: 'Nanopolypyrrole supercapacitor arrays prepared by layer-by-layer assembling method in anodic aluminum oxide templates', *J. Solid State Electrochem.*, 2005, **11**, 32–37.
17. A. Sumboja, X. Wang, J. Yan and P. S. Lee: 'Nanoarchitectured current collector for high rate capability of polyaniline based supercapacitor electrode', *Electrochim. Acta*, 2012, **65**, 190–195.
18. P. Simon and Y. Gogotsi: 'Materials for electrochemical capacitors', *Nat. Mater.*, 2008, **7**, 845–854.
19. W. Wei, X. Cui, W. Chen and D. G. Ivey: 'Manganese oxide-based materials as electrochemical supercapacitor electrodes', *Chem. Soc. Rev.*, 2011, **40**, 1697–1721.
20. S. Giri, D. Ghosh, A. P. Kharitonov and C. K. Das: 'Study of copper ferrite nanowire formation in presence of carbon nanotubes and influence of fluorination on high performance supercapacitor energy storage application', *Funct. Mater. Lett.*, 2012, **05**, 1250046.
21. H. Xia, D. Zhu, Z. Luo, Y. Yu, X. Shi, G. Yuan and J. Xie: 'Hierarchically structured Co_3O_4@Pt@MnO_2 nanowire arrays for high-performance supercapacitors', *Sci. Rep.*, 2013, **3**, 2978.
22. S. Iijima: 'Helical microtubules of graphitic carbon', *Nature*, 1991, **354**, 56–58.
23. D. H. Robertson and D. W. Brenner: 'Energetic of nanoscale graphic tubules', *Phys. Rev. B*, 1992, **45B**, 592–595.
24. L. Ainsworth and C. Vela: 'New one-dimensional conductors: graphitic microtubules', *Phys. Rev. Lett.*, 1992, **68**, 1579–1581.
25. P. Kim, L. Shi, A. Majumdar and P. McEuen: 'Thermal transport measurements of individual multiwalled nanotubes', *Phys. Rev. Lett.*, 2001, **87**, 215502.
26. S. B. Ma, K. W. Nam, W. S. Yoon, X. Q. Yang, K. Y. Ahn, K. H. Oh and K. B. Kim: 'Electrochemical properties of manganese oxide coated onto carbon nanotubes for energy-storage applications', *J. Power Sources*, 2008, **178**, 483–489.
27. H. Xia, Y. Wang, J. Lin and L. Lu: 'Hydrothermal synthesis of MnO_2/CNT nanocomposite with a CNT core/porous MnO_2 sheath hierarchy architecture for supercapacitors', *Nanoscale Res. Lett.*, 2012, **7**, 33.
28. J. Yan, Z. Fan, T. Wei, J. Cheng, B. Shao, K. Wang, L. Song and M. Zhang: 'Carbon nanotube/MnO_2 composites synthesized by microwave-assisted method for supercapacitors with high power and energy densities', *J. Power Sources*, 2009, **194**, 1202–1207.
29. Y. Wang, H. Liu, X. Sun and I. Zhitomirsky: 'Manganese dioxide–carbon nanotube nanocomposites for electrodes of electrochemical supercapacitors', *Scr. Mater.*, 2009, **61**, 1079–1082.
30. A. L. M. Reddy, M. M. Shaijumon, S. R. Gowda and P. M. Ajayan: 'Multisegmented Au–MnO_2/carbon nanotube hybrid coaxial arrays for high-power supercapacitor applications', *J. Phys. Chem. C*, 2009, **114C**, 658–663.
31. L. Hu, W. Chen, X. Xie, N. Liu, Y. Yang, H. Wu, Y. Yao, M. Pasta, H. N. Alshareef and Y. Cui: 'Symmetrical MnO_2–carbon nanotube–textile nanostructures for wearable pseudocapacitors with high mass loading', *ACS Nano*, 2011, **5**, 8904–8913.
32. H. Cheng, A. D. Su, S. Li, S. T. Nguyen, L. Lu, C. Y. H. Lim and H. M. Duong: 'Facile synthesis and advanced performance of $Ni(OH)_2$/CNTs nanoflake composites on supercapacitor applications', *Chem. Phys. Lett.*, 2014, **601**, 168–173.
33. X. Jin, W. Zhou, S. Zhang and G. Z. Chen: 'Nanoscale microelectrochemical cells on carbon nanotubes', *Small*, 2007, **3**, 1513–1517.
34. H. Xia, M. Lai and L. Lu: 'Nanoflaky MnO_2/carbon nanotube nanocomposites as anode materials for lithium-ion batteries', *J. Mater. Chem.*, 2010, **20**, 6896.
35. A. Gaillot, B. Lanson and V. Drits: 'Of birnessite obtained from decomposition of permanganate under soft hydrothermal conditions. 1. Chemical and structural evolution as a function of temperature', *Chem. Mater.*, 2005, **17**, 2959–2975.
36. X. Xie and L. Gao: 'Characterization of a manganese dioxide/carbon nanotube composite fabricated using an in situ coating method', *Carbon*, 2007, **45**, 2365–2373.
37. A. D. Su, X. Zhang, A. Rinaldi, S. T. Nguyen, H. Liu, Z. Lei, L. Lu and H. M. Duong: 'Hierarchical porous nickel oxide–carbon nanotubes as advanced pseudocapacitor materials for supercapacitors', *Chem. Phys. Lett.*, 2013, **561–562**, 68–73.
38. D. P. Dubal, G. S. Gund, C. D. Lokhande and R. Holze: 'Decoration of spongelike $Ni(OH)_2$ nanoparticles onto MWCNTs using an easily manipulated chemical protocol for supercapacitors', *ACS Appl. Mater. Interfaces*, 2013, **5**, 2446–2454.
39. Y. Wang, H. Wang and X. Wang: 'The cobalt oxide/hydroxide nanowall array film prepared by pulsed laser deposition for supercapacitors with superb-rate capability', *Electrochim. Acta*, 2013, **92**, 298–303.
40. S. Vijayakumar, A. K. Ponnalagi, S. Nagamuthu and G. Muralidharan: 'Microwave assisted synthesis of Co_3O_4 nanoparticles for high-performance supercapacitors', *Electrochim. Acta*, 2013, **106**, 500–505.
41. P. X. Hou, C. Liu and H.-M. Cheng: 'Purification of carbon nanotubes', *Carbon*, 2008, **46**, 2003–2025.